

Coupled-cluster approach to Coster-Kronig decay and Auger decay in hydrogen sulfide and argon

Jan Philipp Drennhaus, Anthuan Ferino-Pérez,
Florian Matz, and Thomas-C. Jagau

E-Mail: thomas.jagau@kuleuven.be

Department of Chemistry, KU Leuven, B-3001 Leuven, Belgium

February 28, 2024

Abstract

We perform *ab initio* simulations of the total and partial Auger decay widths of $1s^{-1}$, $2s^{-1}$ and $2p^{-1}$ ionized hydrogen sulfide and $2s^{-1}$ ionized argon with non-Hermitian quantum chemistry. We use coupled cluster theory with single and double substitutions (CCSD) and equation of motion CCSD (EOM-CCSD) and discuss the novel application of (equation of motion-) second order Møller-Plesset perturbation theory (MP2). We find good agreement between the methods for the $1s^{-1}$ hole of H_2S , whereas for the other holes we can only use the EOM methods. We obtain very large decay widths of the $2s^{-1}$ -vacant states due to intense Coster-Kronig transitions with excellent agreement to experiments. The three $2p^{-1}$ holes show completely different spectra because a decay channel is only significant when one of the final holes is spatially aligned with the initial hole. Lastly, we observe that triplet channels are much more important for the $2s^{-1}$ and $2p^{-1}$ holes than for the $1s^{-1}$ hole, for which it is well known that triplet channels only contribute weakly to the total Auger intensity.

1 Introduction

The Auger-Meitner effect[1, 2] is the dominant relaxation mechanism of core-vacant states of light elements, i.e., nuclei lighter than about germanium for K-shell holes and lighter than about neptunium for L-shell holes. This is equivalent to an ionization energy range of up to 13 keV[3–5]. Auger decay is an autoionization of atoms or molecules via emission of Auger electrons, driven by the simultaneous filling of the core-hole. Core-vacant states are not only byproducts of irradiation with X-rays[2, 6, 7], collisions with high-energy particles such as electrons[8], or electron capture[9]. They can also be specifically prepared and analyzed, which gives rise to site- and energy-specific spectroscopic methods to extract a variety of chemical information from molecules[10–19], clusters[20], and materials[12, 21–23] including surfaces[22, 24–28] and nanostructures[29, 30]. Auger electrons are also relevant for radiomedicinal approaches.[31–38]

In these contexts, a specific interest lies in core-holes localized on atoms from the third or higher period of the periodic table because these exhibit more than one shell of core electrons.[9, 12, 14, 18, 20, 22, 25, 27–38] The different core electrons can be selectively ionized since they are well-separated in energy, which gives rise to specific Auger spectra. Further complexity is added because also the electrons involved in Auger electron can stem from different shells. In Auger decay, the respective spectra are dubbed according to the shells of the participating electrons. The first letter describes the initial hole, while the other two letters correspond to the final holes. A *KLL* spectrum, for example, includes channels where a vacancy in

the K shell (1s) gets filled by an electron from the L shell (2s and 2p) while an electron from the same shell gets emitted.

In Coster-Kronig decay, one of the refilling electrons stems from the same shell as the initial core-hole[39]. This manifests in the emission of very slow Auger electrons. An example for Coster-Kronig decay is an LLM decay process where a 2p electron refills a 2s hole, and a electron from the M - shell is emitted. Because of the high orbital overlap, this is much more efficient than intrashell Auger decay and one observes extraordinarily short lifetimes for s-type holes than for those of higher angular momenta within the same shell.[3] These processes are to be distinguished from decay holes in an inner subshell of the outermost electron shell, which can only decay by ionization of the environment[40–43].

Auger decay involving other shells than the valence shell can leave the system with enough energy to undergo further Auger decay instead of vibrational or radiative relaxation. This behavior is typically referred to as a decay cascade and amplifies the number of Auger electrons produced from a single core-ionization, which is desirable for applications in radiotherapy[35]. Decay cascades also leave signatures in Auger decay spectra when the spectra of the original core-ionized state and the primary decay products overlap.[21]

Computational simulation of Auger decay is often a necessary supplement to experiments because it allows definitive assignments of signals to channels and electronic configurations.[17, 18, 44] An important feature of core-vacant states is that Auger decay makes them unbound. Such electronic resonances, i. e. all states which undergo autoionization, require special quantum-mechanical methods to describe the coupling to the continuum.[45–47]

One can distinguish between methods which only aim to compute the energy of Auger decay channels, with which a spectrum can only be constructed when assuming every decay channel to have an identical intensity, and methods where the decay channels' intensities are explicitly calculated which allows prediction of peak shapes in spectra. If only the energy of the core-ionized state is necessary, the core-valence separation (CVS) is often applicable and core-valence (Auger) transitions that make the system unbound are removed from the excitation manifold.[48–59] This method reaches its limits where the energetic separation between the orbital group defined as core within these methods, where the initial hole is located and the one defined as valence, which is involved in Auger decay, is low, as for example in the presence of Coster-Kronig transitions. Also, assuming decay channels of equal intensity is a bad approximation in systems involving more than two shells as the intensities of these bands typically differ strongly.

To explicitly account for the decay process and compute probabilities for each of the decay channels (expressed as partial widths), different methods have been proposed, such as R-matrix theory[60–62] or Fano's theory[63–72], which require explicit descriptions of the final states of the system and the emitted electron. We follow a different approach here, where the outgoing electron is rather described implicitly through complex scaling the coordinates in the Hamiltonian[45, 73, 74] or the basis functions[75, 76] without a need to partition the Hilbert space. This scaling has the effect that the continuum wave functions become L^2 integrable and can therefore be treated by standard quantum chemical methods[46, 77–86]. The other effect is that the eigenenergies become complex, where the imaginary part relates to the decay width of the respective state which is inversely proportional to the life time. The partial widths are extracted via the decomposition of the complex coupled-cluster with singles and doubles (CCSD) energy[46] or by applying Auger channel projectors on the equation-of-motion ionization potential (EOMIP)-CCSD wave function.[84]

Prior applications of the CCSD and EOMIP-CCSD methods, combined with complex scaling of the Hamiltonian or the basis functions, only considered atoms and molecules comprising elements from the first and second row like neon[46, 84], water[46, 84], molecular nitrogen[46], benzene[46, 86] or other hydrocarbons[84, 85]. Here, we apply this method to heavier elements. Our main focus laid on hydrogen sulfide because of its similarity to water and the exhaustive experimental and theoretical literature available.[87–94]

We also investigated the argon atom as a simpler system which allows for a more thorough benchmarking. Both systems have five core orbitals (1s, 2s, 3×2p) which are atom-like and do not participate in bond formation. Thus, five different core holes exist for each of the systems which differ in decay width and spectral shape.

In addition to the computation of Auger decay widths, partial widths, and spectra, we compare the results to the water molecule regarding the spectral shape, the distribution of the decay among the decay channels and the relative contribution of triplet channels to the decay width. We also propose the use of the faster but less exact methods MP2 and EOMIP-MP2 which are based on a perturbational treatment of the correlation in the reference wave function.

This manuscript is structured as follows: In section II, the theory of complex scaling and complex basis functions, (EOM-)MP2 and (EOM-)CCSD, and decomposition and Auger channel projectors will be discussed. We also explain how we obtain the positions and widths of the peaks in the spectra. In section III, we will introduce the systems of interest H₂S and Ar, before we discuss the computational details in section IV. In section V, we present the ionization energies, total Auger decay widths, and lastly the partial decay widths and some spectra. The manuscript will be concluded with an outlook in section VI.

2 Theoretical description of Auger decay

Core-vacant states are electronic resonances and thus not bound but metastable. They can undergo Auger decay and are therefore coupled to the continuum. Continuum wave-functions are not L^2 integrable, as they approach a plane wave at infinity, which poses a major challenge to standard computational methods.

The approaches used throughout the article to describe the resonance character of core-ionized states are based on complex scaling or complex basis functions. Extensive discussion of the description of core-vacant states using these methods can be found elsewhere.[46, 47, 84] Hereafter we delineate the aspects of the theory relevant to our work.

Complex scaling and complex basis functions

Complex scaling[73] (CS) of the Hamiltonian \hat{H} describes the following similarity transformation

$$\hat{H}_{\text{CS}} = \hat{S}\hat{H}\hat{S}^{-1}, \hat{S} = e^{i\theta r \frac{d}{dr}}, \theta \in \left(0, \frac{\pi}{4}\right). \quad (1)$$

The effect of this on the energy of the continuum wave functions is a rotation with an angle 2θ into the lower half of the complex plane. The resonance states become L^2 integrable, given θ is larger than a critical angle θ_c which is in the order of 0.01° for Auger decay in neon.[46] The eigenenergies of the resonances E_{res} become complex due to the transformation

$$E_{\text{res}} = E_{\text{R}} - i\frac{\Gamma}{2}. \quad (2)$$

Here E_{R} is the resonance position and Γ the total decay width of that state, which is related to the lifetime τ by $\Gamma = \frac{\hbar}{\tau}$, where \hbar is the reduced Planck's constant. When the Schrödinger equation is treated exactly, E_{res} is independent on θ as long as $\theta > \theta_c$. Due to the finiteness of practical basis sets E_{res} does depend on the scaling angle θ . For this reason, one performs calculations for all possible angles, here in steps of 10 mrad, and minimizes $|\frac{d\Delta E}{d\theta}|$ because this derivative should be zero with a complete basis set. Here, ΔE is the energy difference of the ground and core-vacant state.

CS has the major flaw that it cannot be used to model molecular systems as it is not compatible with the Born-Oppenheimer approximation.[46, 47] Therefore we can only use it for argon. To describe the Auger decay of H₂S we use the method of complex basis functions (CBFs)[75] which is based on the identity

$$\frac{\langle \psi(r) | \hat{H}(re^{i\theta}) | \psi(r) \rangle}{\langle \psi(r) | \psi(r) \rangle} = \frac{\langle \psi(re^{-i\theta}) | \hat{H}(r) | \psi(re^{-i\theta}) \rangle}{\langle \psi(re^{-i\theta}) | \psi(re^{-i\theta}) \rangle}. \quad (3)$$

Here, we do not scale the Hamiltonian (left-hand side) but the coordinates of the basis functions (right-hand side). This has the same effect on the L^2 integrability of the resonance wave functions and the eigenenergies. To preserve the dilation analyticity, we only complex scale some additional diffuse basis functions to describe the emitted electron. To note that we add m complex-scaled shells of azimuthal quantum number l to our basis we add an appendage $+m(l)$ to the name of our basis set. For example, when we add four shells of s , p , and d type, we write $+4(\text{spd})$. In CBF calculations we optimize θ in steps of 1° .

(Equation of motion-)coupled cluster and second-order Møller-Plesset perturbation theories

Coupled-cluster theory in the singlet and doubles approximation (CCSD) was used to study the electronic structure of the systems of interest.[95] Two approaches were then used to describe the core-ionized states. In the first one, two subsequent complex energy CCSD calculations were separately done for the neutral and core-vacant state of the system. We then take the difference of the real energies as the ionization energy and the difference of the imaginary part as the negative half of the decay width.[46] The imaginary part of the ground state is a computational artifact, as for a complete basis set it should be zero. With this approach, we aim to subtract this nonphysical decay width from the total width.

The second approach used was equation-of-motion (EOM)[96–98] ionization potential (IP) CCSD. Here, one acts with an operator

$$\hat{R}^{\text{IP}} = \sum_i^{\text{occ}} r_i i + \frac{1}{2} \sum_{ij}^{\text{occ}} \sum_a^{\text{virt}} r_{ij}^a a^\dagger j i \quad (4)$$

on the CCSD ket of the neutral molecule which introduces 1-hole (i) and 2-hole-1-particle ($a^\dagger j i$) excitations with amplitudes r_i and r_{ij}^a , respectively. The core-hole state is then described as

$$|\Psi_{\text{EOM-IP-CCSD}}\rangle = \hat{R}^{\text{IP}} |\Psi_{\text{CCSD}}\rangle = \hat{R}^{\text{IP}} e^{\hat{T}} |\Phi_{\text{HF}}\rangle. \quad (5)$$

More details on the CCSD and EOM-CCSD approaches for the treatment of electronic resonances can be found elsewhere.[47, 83, 95] Furthermore, in this work, we also explore the performance of second-order Møller-Plesset perturbation theory (MP2) in describing Auger decay for different core-holes. Analogous procedures to the ones presented for CCSD were carried out for the description of the core-holes within MP2.[99]

Partial decay widths

As in Auger decay, usually, a variety of final states are possible, we are interested in how the total decay width (Γ) splits up in these individual decay channels. Since the partial width divided by the total width equals the relative probability that the resonance decays via the respective channel, the partial decay widths can be used as a proxy for the intensity of Auger decay channels. Two different methods have been proposed in the scope of the CS/CBF treatment of Auger decay.

The first approach is based on an energy decomposition analysis which only gave good results for CCSD and not for EOM-CCSD in previous projects.[46] We therefore only use it for the CCSD and MP2 calculations. For a fixed initial core-hole a , the decay channel is defined by the two holes i and j in the occupied part of the final state. Note again that the decay width is twice the negative imaginary part of the complex energy. Thus, the partial decay width for CCSD is given by

$$\gamma_{ij}^{\text{CCSD}} = -2 \text{Im} \left(\sum_b^{\text{virt}} \left(2t_i^a t_j^b + t_{ij}^{ab} \right) \langle ab || ij \rangle \right). \quad (6)$$

Here we sum over all virtual orbitals b that describe the emitted electron. As the two-electron integrals $\langle ab || ij \rangle$ are automatically computed in any CCSD and MP2 calculation the computation of the partial widths does not bring much additional computational cost. From equation (6) it is possible to derive an expression for γ_{ij} when MP2 is used instead of CCSD. The partial decay width of a particular channel is then given by

$$\gamma_{ij}^{\text{MP2}} = -2 \text{Im} \left(\sum_b^{\text{virt}} \frac{\langle ab || ij \rangle^2}{\epsilon_a + \epsilon_b - \epsilon_i - \epsilon_j} \right). \quad (7)$$

Within this approximation the Γ_{ij} of a specific channel can be calculated without the need of perform a full energy calculation since only certain integrals are needed. This has the small caveat that the optimal θ still need to be optimized.

For the EOM-MP2 and EOM-CCSD calculations, the Auger channel projector (ACP) approach was used.[84] Here one excludes the determinants corresponding to a specific Auger decay channel from the excitation manifold. By analyzing the effect of this on the complex energy in comparison to the full excitation manifold, one obtains the partial decay width of the respective channel. As this has to be repeated for every decay channel the ACP approach is usually computationally more expensive than the decomposition analysis. We therefore only use it for the EOM methods, where the decomposition method gave bad results in previous projects.[46]

Positions and broadening of the peaks in the spectra

To simulate an Auger spectrum we need not only the partial widths (the height of the peaks) but also the broadening of the peaks and the kinetic energy of the respective emitted electron (the position of the peak). We calculate the latter by comparing the energy of the core-vacant state, which we get from a real EOM-IP-CCSD calculation, with the energy of the respective doubly ionized state. The latter is calculated by a real EOM double ionization potential (DIP-)CCSD calculation,[100–102] which is equivalent to EOM-IP-CCSD with the difference that the operator \hat{R} now introduces 2-hole and 3-hole-1-particle excitations

$$\hat{R}^{\text{DIP}} = \frac{1}{2} \sum_{ij}^{\text{occ}} r_{ij} j i + \frac{1}{6} \sum_{ijk}^{\text{occ}} \sum_a^{\text{virt}} r_{ijk}^a a^\dagger k j i. \quad (8)$$

The DIP states can be composed of multiple decay channels. We then assign to these states a sum of decay widths, where the weighting factors are given by the relative squared amplitudes of the channel to that state. This procedure has successfully been used in previous projects.[86] All relevant DIP states can be found in the supplementary material.

In experiments, the kinetic energy of emitted electrons cannot be measured perfectly. Different mechanisms lead to a broadening of the spectral lines like lifetime broadening, Doppler broadening, or pressure broadening. Depending on which mechanisms dominate, the lines show Gaussian (Doppler) or Lorentzian

(lifetime and pressure) profiles. As the broadening, for some part, depends on the respective experiment, there is no *a priori* optimal way to model the peak widths. We therefore adjust ourselves by the experiments that we want to compare our computations to and choose either Gaussian or Lorentzian and the full width at half maximum (FWHM) to match the experimental line shapes as well as possible.

3 Electronic structure of hydrogen sulfide and argon

Neutral hydrogen sulfide has 18 electrons, just like the noble gas argon. H_2S belongs to the C_{2v} molecular point group, which has the four irreducible representations a_1 , a_2 , b_1 , and b_2 . Its electronic configuration is $(1a_1)^2(2a_1)^2(1b_1)^2(3a_1)^2(1b_2)^2(4a_1)^2(2b_1)^2(5a_1)^2(2b_2)^2$. Here, we use the Q-Chem symmetry notation instead of the traditional Mulliken’s notation. The first five orbitals are effectively atom-like as they represent the sulfide’s 1s, 2s, and 2p orbitals. Plots of all occupied orbitals can be found in the supplementary material.

The argon atom also with 18 electrons belongs to the $\text{SO}(3)$ molecular point group. Its electronic configuration is $(1s)^2(2s)^2(2p)^6(3s)^2(3p)^6$. All argon calculations were carried out in D_{2h} , the largest Abelian subgroup of $\text{SO}(3)$.

4 Computation details

The geometry of the H_2S molecule was optimized using the resolution-of-the-identity MP2 method[103], the aug-cc-pCVTZ basis and the riMP2-aug-cc-pCVTZ auxiliary basis sets. We found a bond length of 1.334 and an angle of 92.205° in good agreement with the reported results.

All complex energy calculations of H_2S were carried out using the aug-cc-pCVTZ(5sp) basis for sulfur and aug-cc-pVTZ(5sp) basis for hydrogen. These basis sets were built by substituting the s and p exponents of the aug-cc-pCVTZ basis with those from the aug-cc-pCV5Z basis. This procedure has shown good results in previous projects.[46, 84] The exponents of the added complex-scaled shells were calculated by scaling the optimized values to Ne[84] with respect to the geometric mean $\bar{\zeta}$ of the exponents in the aug-cc-pCVTZ(5sp) basis set.[46] We found $\bar{\zeta} = 5.50, 3.02$, and 0.42 for Ne, S and H, respectively. Therefore we scale the exponents of Ne by a factor 0.550 and 0.076 for S and H, respectively.

In calculations where we went beyond four complex-scaled shells per angular momentum, we produced additional exponents by adding even-tempered exponents to the basis set. Furthermore, when the initial core hole is in one of the three 2p-like orbitals, one should theoretically need f-type CBFs.[104] We obtained them for sulfur by taking the exponents from the d-type functions and scaling them with a factor 0.8 as this is also roughly the factor between d- and f-type exponents in the aug-cc-pVTZ(5sp) basis set. The final basis set can be found in the supplementary material.

In the case of argon, the full aug-cc-pCV5Z basis set was used in order to have enough an appropriate basis set for the complex scaling method. The exponents for the CBF calculations were calculated in the same way as for hydrogen and sulfur ($\bar{\zeta}_{\text{Ar}} = 2.80$) and can also be found in the supplementary material.

The energy of the initial core-ionized and the final double ionized states were calculated using also the aug-cc-pVTZ(5sp) basis set. However, we were not able to converge any state that involved the $2a_1^{-1}$ ($2s^{-1}$) hole of H_2S with a real EOM-IP or EOM-DIP calculation. For that reason, in the case of the IP energy of the $2s^{-1}$ state we took the real part of the complex EOM-IP-CCSD energy. The missing energies of the doubly ionized states were calculated using an extrapolation procedure. We first computed the energy of all doubly ionized states with a reduced operator $\hat{R}^{\text{DIP, red}} = \frac{1}{2} \sum_{ij}^{\text{occ}} r_{ij} j i$ that only involves 2-hole excitations, which converges for every state. We then compare, for the states where the calculation with the non-reduced \hat{R}^{DIP} converged, the obtained energies with full or reduced excitation manifold. Subsequently, we calculated the correlation energy as a function of the energy obtained with the $\hat{R}^{\text{DIP, red}}$ calculation. We linearly extrapolate

Table 1: Ionization energies of the studied core holes.

Core hole	Ionization energy/eV	Experiment
H ₂ O 1s ⁻¹	541.42	538.728 ± 0.017[106]
H ₂ S 1s ⁻¹	2475.75	2478.25 ± 0.40[88]
H ₂ S 2s ⁻¹	234.99	235 ± 0.1[90]
H ₂ S 1b ₁ ⁻¹	171.95	Not measurable
H ₂ S 1b ₂ ⁻¹	171.83	Not measurable
H ₂ S 3a ₁ ⁻¹	171.78	Not measurable
Ar 1s ⁻¹	3198.85	3206.3 ± 0.3[107]
Ar 2s ⁻¹	326.58	326.25 ± 0.05[108]

this to get the approximate correlation energy for the missing states. The extrapolation procedure for all the missing energies can be found in the supplementary material. In the case of argon, it was only possible to converge some of the doubly ionized states that include a 2s⁻¹ hole. For the missing energies, we applied the same procedure as for H₂S.

All calculations were performed on a modified version of the Q-Chem program package.[105]

5 Results

5.1 Core ionization energies

Table 1 shows the ionization energies (IEs) of the different core holes studied in this work. The given values are the real parts of the energies from complex EOM-IP calculations. We used for H₂O +2(sp), for H₂S 1s⁻¹ +4(sp), for H₂S 2s⁻¹ +8(sp), for the H₂S 2p⁻¹ states +4(sp) and for Ar 2s⁻¹ +8(sp).

The comparison of the theoretical IEs computed for the studied systems with the experimental data, when available, reveals that the biggest discrepancies occur for the 1s core holes. In the case of water, the energies are higher by ~1 eV, while for H₂S and Ar, the differences are around 2.5 eV and 6.41 eV respectively. Probably, one of the causes of this increment is the lack of a proper treatment of the relativistic effects that start to be relevant in third-row elements.

5.2 Total Auger decay widths

K-edge Auger decay

The 1s⁻¹ Auger decay in H₂S, was studied using all four methods previously discussed, MP2, CCSD, EOM-MP2, and EOM-CCSD. See table 2 for the optimal θ , the total widths, and the sum of the partial widths for the different methods and number of added complex-scaled shells. We find good agreement between the methods in the total width and the sum of partial widths with two complex-scaled shells per angular momentum except for EOM-CCSD. For the latter case, we went to four shells to get a better agreement with the other methods in the sum of partial widths. For the CCSD method, we found that going to four shells is not needed. Our calculated total width varies between 419 and 490 meV between the methods, whereas the sum of partial widths varies between 400 and 448 meV. There are multiple reasons for the discrepancy between total width and sum of partial widths.[46, 84] Probably the most important is that the decomposition and ACP methods do not account for excited determinants that relate to shake-up and shake-off processes, which do contribute to the total width. The calculated values lay inside the error bars of the experimental value.[109] The semi-empirical theoretical value from Krause and Oliver[110] lays about

Table 2: Optimal angle θ_{opt} , total width, and the sum of partial widths (p.w.) of $1s^{-1}$ Auger decay of hydrogen sulfide computed with different methods and number of complex-scaled shells.

Method	CBFs	θ_{opt} [$^{\circ}$]	Total width [meV]	Sum of p.w. [meV]
CCSD	+2(spdx)	30	443.6	446.6
CCSD	+4(spdx)	14	436.1	451.8
EOM-CCSD	+2(spdx)	40	419.2	276.0
EOM-CCSD	+4(spdx)	16	430.6	399.8
MP2	+2(spdx)	40	484.1	448.1
EOM-MP2	+2(spdx)	19	490.7	430.7
Theory[110]			590	
Theory (only KLL)[87]			430	
Experiment[109]			500 \pm 100	

Table 3: Optimal angle θ_{opt} , total width and sum of partial widths (p.w.) of the $2s^{-1}$ Auger decay of hydrogen sulfide calculated with EOM-CCSD and +4(spdx), +6(spdx) and +8(spdx).

Method	CBFs	θ_{opt} [$^{\circ}$]	Total width [meV]	Sum of p.w. [meV]
EOM-CCSD	+4(spdx)	17	1119.1	1020.0
EOM-CCSD	+6(spdx)	27	1603.2	1407.4
EOM-CCSD	+8(spdx)	14	1672.2	1440.5
Experiment[90]			1800	
Theory[110]			1490	

40% higher but is calculated with a much weaker theory. The theoretical value from Faegri and Keski-Rahkonen[87] is interpolated from a calculation from Chen and Crasemann[111] but only includes the *KLL* Auger decay. The *KLL* part of the spectrum makes up between 87% and 89% of the total width in our calculations, dependent on the method. Our values for the *KLL* part of the sum of partial width thus lie between 347 meV and 400 meV.

L₁-edge Auger decay

The description of the Auger decay process that occurs as a result of a vacancy in the $2a_1$ orbital of hydrogen sulfide is more computationally challenging than that of the K-edge Auger decay. The reason for this is probably that the $2s^{-1}$ state is much more correlated than the $1s^{-1}$ state, due to the energetic proximity of the $2s$ orbital to the valence orbitals. Hence, CCSD does not converge in this case. Furthermore, MP2 gave very bad results as the total width increased from 0.526 to 19.5 eV, when going from two to five shells per angular momentum. Therefore we only consider calculations with EOM-CCSD. We performed calculations with four, six, and eight complex-scaled shells per angular momentum. The first addition of CBFs increased the total width considerably and led to a better agreement with an experimental and another theoretical value, as can be seen in Table 3. Using eight instead of six shells increased the decay width again, but had a much smaller impact. The need for more diffuse CBFs can be explained by the low energy of the emitted electrons. Additionally, we observed that EOM-MP2 gives very similar results with almost no computational benefit.

Table 4: Optimal angle θ_{opt} , total width, and the sum of partial widths (p.w.) of the $2s^{-1}$ Auger decay of argon.

Method	CBF/Basis	θ_{opt} [$^{\circ}$]	Total width [meV]	Sum of p.w. [meV]
CS-EOM-CCSD	5Z	17 $^{\circ}$	2632.3	2450.2
CS-EOM-CCSD	QZ	16 $^{\circ}$	2531.8	2347.3
CS-EOM-MP2	5Z	16 $^{\circ}$	2620.8	2382.0
CBF-EOM-CCSD	+4(spd)	14 $^{\circ}$	1053.8	872.2
CBF-EOM-CCSD	+6(spd)	32 $^{\circ}$	2100.9	2294.6
CBF-EOM-CCSD	+8(spd)	34 $^{\circ}$	2668.6	2334.2
Experiment[108]			2250 \pm 150	
Experiment[108]			2250 \pm 50	
Experiment[113]			1840 \pm 200	
Theory[108]			1850.0	
Theory (only LLM)[114]			2330.0	
Theory[110]			1630	

The total width is almost four times as large as for the $1s$ hole even though fewer decay channels exist. The reason for that is the existence of very intense Coster-Kronig[39] transitions where an electron of the same shell fills the hole and a valence electron with relatively little kinetic energy gets emitted. Here, a $2p$ electron fills the $2s^{-1}$ hole, which are the *LLM* transitions. Those decays happen so fast because the $2s$ and $2p$ orbitals have very large radial overlap.[112] The *LLM* part makes up 1396 of the total 1441 meV (sum of partial widths with +8(spd)). Interestingly, triplet channels contribute much more to the total width here than for the $1s^{-1}$ hole. The ratio between singlet and triplet channels is 0.76 : 0.24, whereas for $1s^{-1}$ it is 0.95 : 0.05.

The $2s^{-1}$ Auger decay of argon has been investigated much more[108, 113–119] than in the case of H_2S which enables a better comparison for our simulation. An advantage of argon is that we can use complex scaling which is more straightforward as it does not require the optimization of the CBFs' exponents and enables the comparison and therefore verification of the CBF approach. Table 4 shows θ_{opt} , the total width and the sum of partial widths calculated with EOM-CCSD and four, six and eight complex-scaled shells for s , p and d angular momentum, and complex scaling with aug-cc-pCV(Q and 5)Z (EOM-CCSD) and aug-cc-pCV5Z (EOM-MP2). We find that aug-cc-pCVQZ gives a very similar result to the more complete 5Z basis. Also, EOM-MP2 agrees very well with EOM-CCSD but brings almost no time benefit. Furthermore, we find that adding 4(spd) is not enough to describe the process properly. As for H_2S , we see that eight complex scaled shells only slightly change the sum of partial widths compared to six. The agreement between the CS and CBFs calculations is also very good, verifying our calculations for hydrogen sulfide. The values of our best calculated sums of partial widths 2450 meV (CS) and 2334 meV (CBF) also agree very well with the most recent experiment[108] (2250 meV) and theoretical value[114] (2330 meV). The latter only describes the *LLM* part of the spectrum, which contributes 97% of the total sum of widths in our calculations. The older result for the total width is about 20% smaller.

$L_{2,3}$ -edge Auger decay

Auger electrons can also be produced when the core hole is present in one of the three $2p$ -like orbitals of H_2S , namely $1b_1^{-1}$, $3a_1^{-1}$, and $1b_2^{-1}$. Again like for the $2s^{-1}$ hole, the used solver for the CCSD equations

Table 5: Total width and the sum of partial widths (p.w.) in meV for the three 2p holes $1b_2^{-1}$, $3a_1^{-1}$ and $1b_1^{-1}$ and the mixed states $3e_{1/2}^{-1}$, $4e_{1/2}^{-1}$, and $5e_{1/2}^{-1}$ of hydrogen sulfide.

Initial hole	$1b_2^{-1b}$	$3a_2^{-1b}$	$1b_1^{-1b}$	$5e_{1/2}^{-1}$	$2p^{-1c}$		
ϵ_1^{-1}	ϵ_2^{-1}	ϵ_3^{-1}	$2p^{-1c}$				
Total width ^a	86.1	76.7	68.6	76.3	72.4	82.8	77.1
Sum of p.w. ^a	52.4	47.1	38.7	45.4	42.6	50.2	46.0
Experiment[91]				63 ± 1	65 ± 5	75 ± 1	68 ± 2
Experiment[92]				64 ± 2		74 ± 2	69 ± 2
Theory[92]	90.5	69.8	49.7	68	59	83	70
Theory[110]							54

^aComputed with EOM-CCSD/aug-cc-pCVTZ(5sp)+4(spdf).

^b θ_{opt} is 11° , 10° and 10° for $1b_2^{-1}$, $3a_1^{-1}$ and $1b_1^{-1}$, respectively.

^cThe width of $2p^{-1}$ is taken as the average over the three holes.

does not converge and MP2 does not give trustful results. EOM-MP2 again shows almost identical results to EOM-CCSD but does not have much computational benefit. We therefore limit ourselves to the latter method here. There are now three possible holes ($1b_1^{-1}$, $3a_1^{-1}$ and $1b_2^{-1}$) that are almost energetically degenerate (the ionization potentials vary by about 0.1 eV, see table 1).

As mentioned in section III, f-type added shells should now be necessary to describe the Auger decay. We performed multiple calculations for the three holes, with two and four complex-scaled shells per angular momentum and with or without complex-scaled f shells on sulfur. We found that the results with four shells are much better than with two, as we already saw for the $1s^{-1}$ hole. The effect of the added f-type shells is, however, small. The effect may have been larger if we had also added f CBFs to hydrogen and not only to the sulfur basis, although it helped to find a clearer and more pronounced optimal θ in the optimization trajectory. We therefore present the results for this more complete basis. A comparison between the calculations with different methods and basis sets for the $1b_2^{-1}$ hole can be found in the supplementary material.

Due to spin-orbit coupling the three 2p orbitals mix to $2p_{1/2}$ and $2p_{3/2}$ states. The ligand-field effect (the effect of the hydrogen atoms on the core structure of sulfur) splits the latter again. We will call the resulting states $\epsilon_{2,3}$ while the $2p_{1/2}$ states will then be called ϵ_1 . The latter is energetically separated by about 1.2 eV from the other two levels which are split up by about 110 meV.[91, 93] As these energy differences are on the order of magnitude of the lifetime broadening of the respective states, the various hole states overlap leading to lifetime interferences. The ionization that prepares the molecule in the core-vacant state and the Auger decay should therefore be described as a one-step process[91], which is not done here. The mixing of the $1b_1$, $3a_1$ and $1b_2$ orbitals into these ϵ states have been previously reported[92] and can be found in the supplementary material.

Therefore, we were able to compute the decay widths for both types of state descriptions. This is shown in table 5, in comparison with experimental[91, 92] and other theoretical results[92, 110]. We first observe that the width of the $2p^{-1}$ state is one order of magnitude smaller than the $1s^{-1}$ hole and almost two orders smaller than for the $2s^{-1}$ hole. Note however that the L_2MM width of H_2S with 46 meV is much larger than the KMM width (1.3 meV) and of similar size as the L_1MM width (44 meV). The reason is that the 2s and 2p orbitals have much more spatial overlap with the valence electrons than the 1s orbital. Furthermore, the discrepancy between our calculated total width (difference between the imaginary part of the energy of neutral ground state and core-vacant state) and the sum of partial widths obtained by the ACP procedure is

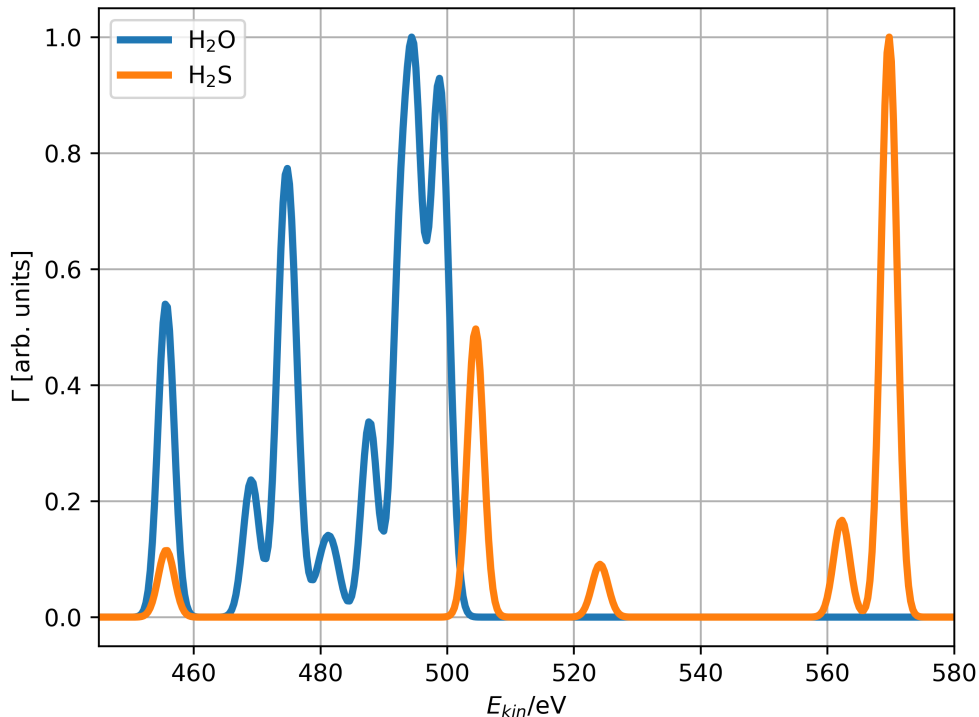


Figure 1: Comparison of the *KLL* Auger spectrum of water and hydrogen sulfide. Decay width in arbitrary units as function of the kinetic energy of the emitted electron. The partial widths were calculated with CCSD and +2(sp). The peaks corresponding to the *KLL* Auger spectrum of H_2S were shifted 1515 meV. All peaks were normalized to ease the comparison. Gaussian broadening with FWHM = 3 eV.

more pronounced on a relative scale than for our previous calculations. The reason behind this is not clear. Although our calculated total widths are too large and our sum of partial widths too small in comparison to the experiments, our results agree well with the experiment that the ϵ_3^{-1} state, which mostly consists of the $1b_2^{-1}$ state, has the largest width. We also reproduce previous theoretical results which report that the width of $3a_1^{-1}$ is larger than that of $1b_1^{-1}$. [92]

5.3 Auger Spectra

K-edge Auger spectra

K-edge Auger spectra have been previously studied for different molecules using the discussed methodology. [46, 70, 84] In particular, the Auger decay of water, an example that has been extensively discussed, is an interesting point of comparison for the *KLL* Auger spectrum of H_2S due to the chemical and electronic similarities between these two molecules. Figure 1 illustrates this comparison. Here we have shifted the *KLL* spectrum of H_2S by 1515 meV to match the lowest energy peak in the spectrum and ease the comparison. All the peaks in the *KLL* Auger spectrum of water can be found in an energy range of less than 50 eV while for H_2S this energy range is ~ 130 eV, which can probably be explained by the difference in the energies between the orbitals in this region. Another significant difference between these two spectra are the number of peaks present in each of them. The Auger spectrum of water shows 7 peaks while in hydrogen sulfide only 5 peaks are visible. This difference can be caused by the fact that, in water, the decay occurs

Table 6: *KLL* partial decay widths in meV of water and hydrogen sulfide molecules.

Decay channels	H ₂ O		H ₂ S	
	Partial width	Relative intensity ^a	Partial width	Relative intensity ^a
2a ₁ — 2a ₁ (S)	16.72	0.96	24.60	0.51
2a ₁ — 3a ₁ (S)	13.48	0.77	35.30	0.74
2a ₁ — 1b ₁ (S)	7.25	0.41	35.30	0.74
2a ₁ — 1b ₂ (S)	12.34	0.71	35.40	0.74
2a ₁ — 3a ₁ (T)	2.44	0.14	6.50	0.14
2a ₁ — 1b ₁ (T)	1.91	0.11	6.50	0.14
2a ₁ — 1b ₂ (T)	2.94	0.17	6.50	0.14
3a ₁ — 3a ₁ (S)	11.65	0.67	35.70	0.75
1b ₁ — 1b ₁ (S)	10.05	0.57	35.50	0.74
1b ₂ — 1b ₂ (S)	16.49	0.94	36.60	0.77
3a ₁ — 1b ₁ (S)	17.49	1.00	47.80	1.00
3a ₁ — 1b ₂ (S)	16.43	0.94	47.00	0.98
1b ₁ — 1b ₂ (S)	14.18	0.81	46.90	0.98
3a ₁ — 1b ₁ (T)	0.16	0.01	0.00	0.00
3a ₁ — 1b ₂ (T)	0.27	0.02	0.00	0.00
1b ₁ — 1b ₂ (T)	0.00	0.00	0.00	0.00

^aCalculated with respect to the most intense width in the region.

from valence orbitals, while in H₂S the orbitals involved retain a certain atomic character which is reflected in the spectrum and the partial widths.

From this figure it becomes clear that spite the chemical resemblances between H₂O and H₂S their Auger decay processes are very different. This conclusion can be further supported by looking at the partial widths for the 16 decay channels of the *KLL* region for these two molecules. These results are presented in Table 6. By looking at the *KLL* partial widths we observe that channels in H₂S are more intense than their counterpart in water with the exception of the three 3a₁—1b₁, 3a₁—1b₂, and 1b₁—1b₂ triplet channels. The relative intensities reveal that in both molecules the 3a₁—1b₁ singlet channel is the most intense of the *KLL* spectrum. However, the relative intensities of the remaining channels exhibit significant variations, notably the pronounced intensity of the 2a₁—2a₁ channel in water, a feature that is less prominent in H₂S.

The widths of all 64 decay channels of H₂S computed with the four methods discussed in this work can be found in the supplementary material. The analysis of these partial widths for the 1s⁻¹ Auger decay of H₂S shows a good agreement between the different methods, but only when using +4(sp) for EOM-CCSD. The agreement between CCSD and MP2 is surprisingly good. The widths of the significant channels only vary between about 1% and 5%. The mean difference between these methods for the channels with a width larger than 1 meV is only 3%.

We will keep focusing our attention on the *KLL* part of the spectrum and compare it with three experimental measurements.[87–89] This is shown in figure 2. We observe five peaks corresponding (from left to right) to the 2s₁⁻² (¹S), 2s⁻¹ 2p⁻¹ (¹P), 2s⁻¹ 2p⁻¹ (³P), 2p⁻² (¹S) and 2p⁻² (¹D) final states, respectively. The intensity in the spectra is normalized to 1 for the highest peak. We only show the CCSD result as a proxy, as all our four methods give similar spectra. Whereas the positions of the peaks agree very well in the experiments, there is some disagreement in our calculation. The highest peak (2p⁻² (¹D)), for example,

lays 13.7 eV higher in energy for the experiment than in our computation. A reason could be that we did not include relativistic effects and spin-orbit splitting in our EOM-CCSD calculations. The major disagreement in the height of the peaks between the experiments and our calculations is that we overestimate the three peaks at lower kinetic energy compared to the other two. The overestimation is the largest for the CCSD and MP2 calculations. An overestimation of peaks at lower kinetic energies was already observed in a previous project with small molecules.[85]

A usual comparison of computed Auger spectra is with the equal width approximation. Here, one assumes that the width equally splits up into all possible channels. The corresponding plot can be found in the supplementary material. The agreement between our calculation and the experiments is very poor. The largest disagreement is that in the equal width approximation, an additional peak to the right of the large $2p^{-2}$ arises stemming from a 3P channel that is forbidden and exactly zero in our calculations. In the experiments, this peak is finite but still very small due to spin-orbit coupling.[88] Lastly, note that except from the $2s^{-1} 2p^{-1}$ (3P) state all triplet channels are negligible in the $1s^{-1}$ calculation. The singlet channels contribute 425 meV of the total sum of widths of 447 meV in the CCSD calculation. This is very similar to the other methods.

While the sum of KLL widths is 400 meV (for our CCSD result), the KLM ($M = \text{valence}$) and KMM contribute 45.7 and 1.3 meV, respectively. The reason that these widths are smaller is that the M electrons have a smaller spatial overlap with the K hole than the L electrons. The respective computed spectra can be found in the supplementary material. To the author's knowledge, there are no experimental results published of those spectra.

L_1 -edge Auger spectra

Figure 3 shows the LLM Auger spectrum starting from the $2a_1^{-1}$ core-ionized state of H_2S . This spectrum consists of 24 of the total 40 decay channels, and it contributes by far the most to the total width. We compare the EOM-CCSD with four, six, and eight complex-scaled shells with the equal widths result. We see two clearly separated structures in the spectrum. Towards lower kinetic energies at about 22.5 eV we see a singular peak which corresponds to the $2p^{-1}4a_1^{-1}$ final states ($L_1L_2M_1$). In our calculations, the corresponding singlet channels are the most intense with 230 meV for the calculation with +8(spd). Note that our calculation produces negative decay widths (~ -10 meV) for the corresponding triplet channels. The reason for this is not totally clear, however, it is certain that our theoretical model misses the spin-orbit coupling that leads to a splitting of the 3P level. The latter lay at a slightly higher energy than the corresponding singlet channel. This is the reason why the peak of equal widths is broader and seems to be shifted to the right.

Towards larger kinetic energies we see a more complex structure consisting of the $18 2p^{-1}M_2^{-1}$ (with $M_2 = 2b_1, 5a_1, 2b_1$) final states ($L_1L_2M_2$). The calculation with four complex shells here also gives some negative widths, which is not the case for six and eight added complex-scaled shells. Our calculated ratio between $L_1L_2M_1$ and $L_1L_2M_2$ is $0.47 : 0.53$ ($\frac{6}{24} : \frac{18}{24}$ for equal widths) for the +8(spd) result. Unfortunately, to our knowledge, an experimental measurement of the LLM spectrum of hydrogen sulfide with sufficient resolution that allows a meaningful comparison with our simulation has not been reported. However, a very noisy $L_1L_2M_2$ spectrum was reported, where three peaks are weakly visible which agrees with our calculations.[90]

The fact that we find some negative decay widths and only poor agreement between the EOM-CCSD result with four complex shells on the one hand, and six and eight complex-scaled shells on the other side, for the $L_1L_2M_2$ part can at least partly be explained by the exponents of the complex shells being not optimized to describe the slow emitted electrons.

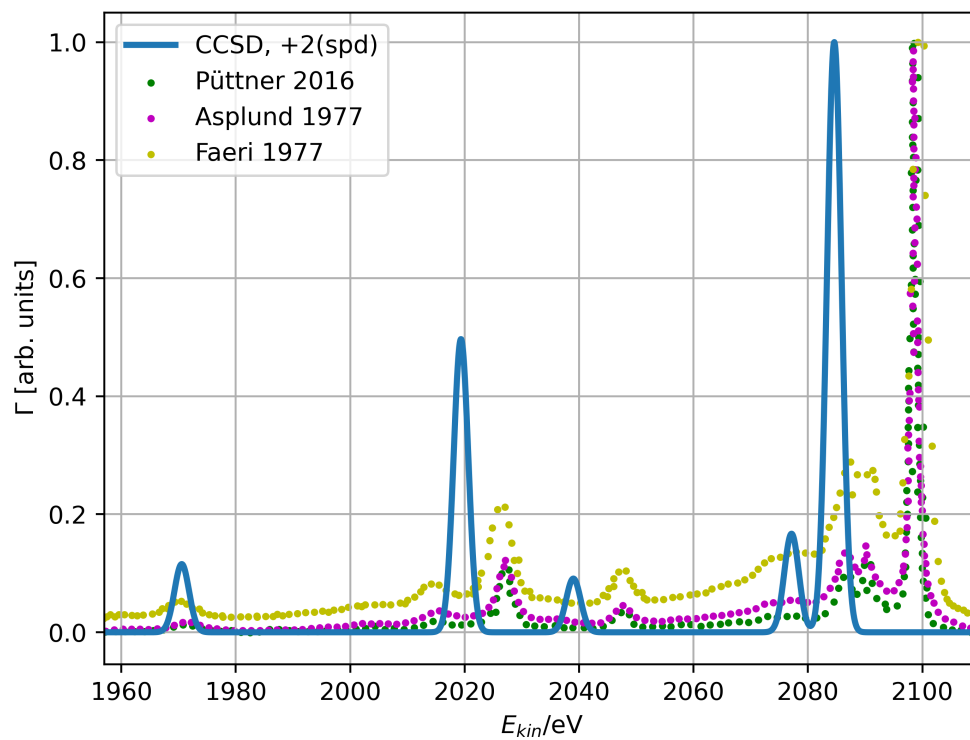


Figure 2: *KLL* Auger spectrum of hydrogen sulfide. Decay width in arbitrary units as function of the kinetic energy of the emitted electron. The blue line shows our result. The partial widths were calculated with CCSD and +2(spd). Gaussian broadening with FWHM = 3 eV.

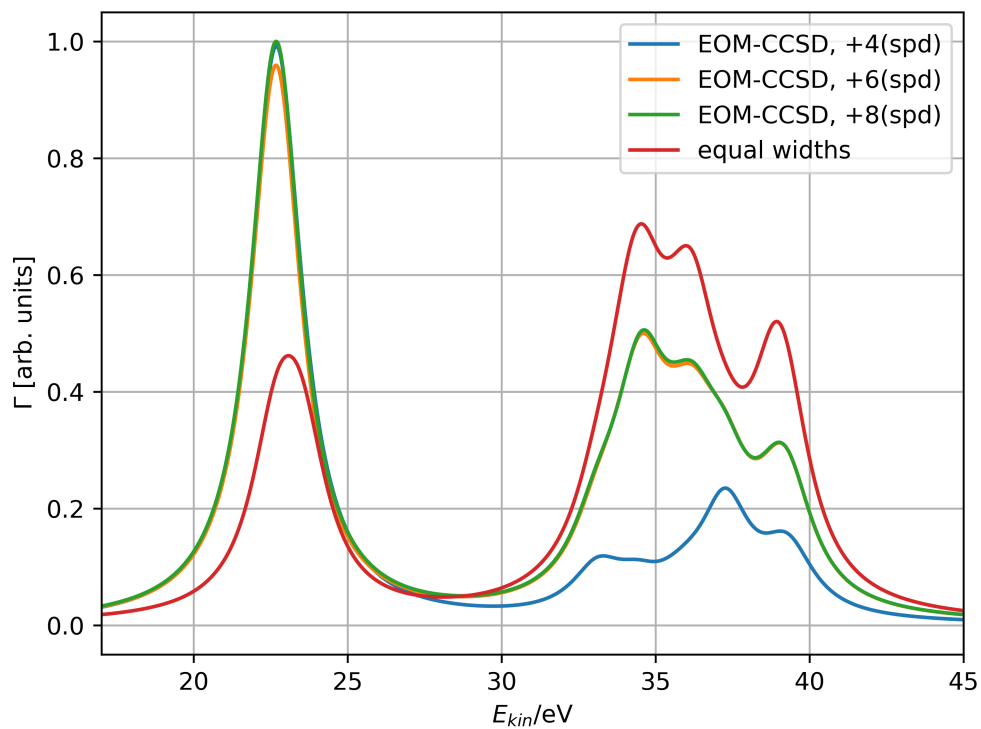


Figure 3: *LLM* Coster-Kronig spectrum of hydrogen sulfide. Decay width in arbitrary units as a function of the kinetic energy of the emitted electron. The partial widths were calculated with CBF-EOM-CCSD. The equal width result is normalized to the same sum of widths as the EOM-CCSD +8(spd) curve. Lorentzian broadening with FWHM = 2 eV.

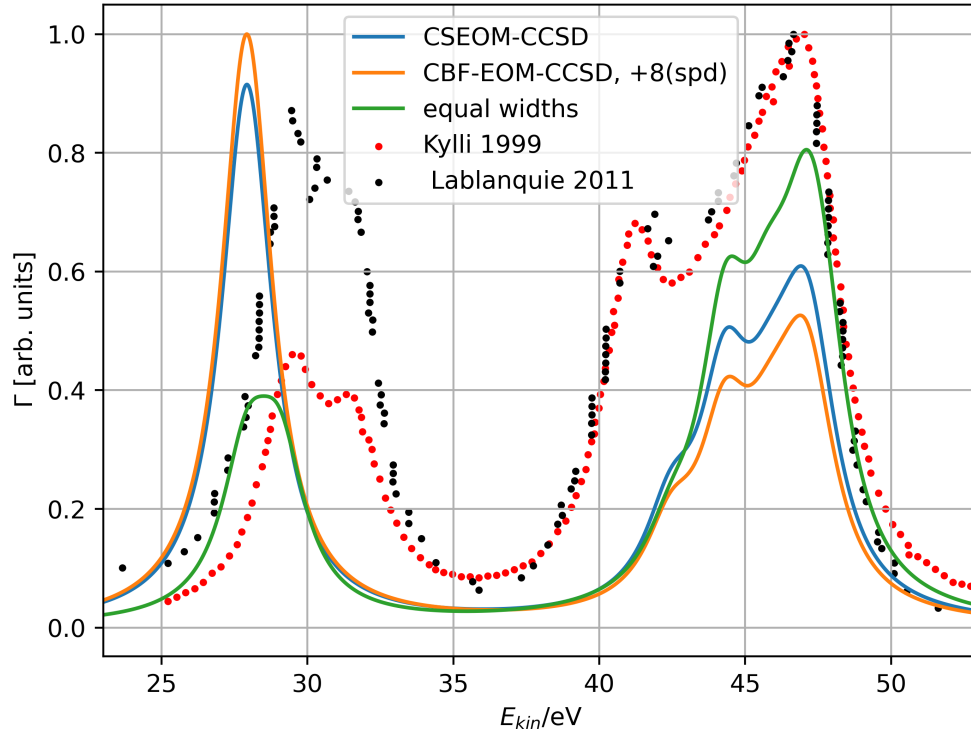


Figure 4: *LLM* Coster-Kronig spectrum of argon. Decay width in arbitrary units as a function of the kinetic energy of the emitted electron. The partial widths were calculated with CS-EOM-CCSD (blue), CBF-EOM-CCSD, and equal widths (green). The calculated spectra are shifted by 3.4 eV towards higher energies to align with the experiments on the rightmost peak. The spectra are normalized to ease the comparison. Lorentzian broadening with FWHM = 2 eV.

The $2s^{-1}$ Auger decay of argon[108, 113–119] has received considerably more attention than H_2S which enables better point of comparison for our methodology. As argon and hydrogen sulfide have a similar core structure the simulated spectra look very similar for the *LLM* part. We can therefore draw conclusions on our H_2S results by comparing our argon calculations with the experiment. The other advantage of argon is that we can use complex scaling which is more straightforward as it does not require the optimization of the CBFs' exponents and enables the comparison and therefore verification of the CBF approach. The partial widths can again be found in the supplementary material. We here focus on investigating the *LLM* spectrum calculated with CS and CBFs which is shown in figure 4. For comparison, an equal width result, which is normalized to the same total width as the CBFs calculation, and two experimental spectra are given. The calculated spectra are shifted to the right such that the rightmost peak aligns with the experiments that are normalized to unity at their highest peak. We first observe the reasonable agreement between the CS and CBFs results. The main difference lies in the partition of the total width between the $L_1L_2M_1$ (around 25 eV) and $L_1L_2M_2$ (around 45 eV). The $L_1L_2M_1:L_1L_2M_2$ splitting is 0.44:0.56 for CS and 0.50:0.50 for CBF, which are similar to the ratio in H_2S . The experimental values for this division are 0.21:0.79[113] and 0.23:0.77[114]. The CS result is in this sense slightly better than CBF. The discrepancy between experiment and calculation for this ratio is long known and have been previously discussed.[114, 120] The authors also observed discrepancies in the $L_1L_2M_1:L_1L_2M_2$ ratio between experiment and theory in the order of a factor 2. They gave multiple possible reasons but most of their computational shortcomings (like electron correlation) are properly accounted for in our calculation. The other reason they give is spin-orbit coupling and the resulting mixing of decay channels. As spin-orbit interaction is completely missing in our calculation, we assume that this is the main reason for the mismatch with experiments. Note, however, that the two shown experiments[114, 115] in figure 4 themselves also disagree in the $L_1L_2M_1:L_1L_2M_2$ ratio.

Furthermore, we see that the $L_1L_2M_1$ part shows a single peak in our calculation. The reason for this is that our calculations give negligible (CS) or even negative (~ -5 meV, CBFs) decay widths for the corresponding triplet channels. This also has a very poor agreement with the experiments that show two peaks, a larger one from the singlet channels and a smaller one from the triplets. The missing of the triplet channels in simulation was also intensively discussed before. The main reason is channel mixing due to spin-orbit coupling which can change the singlet to triplet ratio by as much as a factor 84.[120–122]

We again see also a disagreement in the positions of the peaks compared to the experiment. This is also tied to the missing spin-orbit coupling in the real EOM-IP-CCSD and EOM-DIP-CCSD calculations.

In addition, note that the effect of spin-orbit coupling and channel mixing is not limited to argon or even the Coster-Kronig transitions. We expect that the same effects impair our other results as well. For the $2s^{-1}$ spectrum of hydrogen sulfide, the $L_1L_2M_1$ is most likely also overestimated compared to $L_1L_2M_2$. The missing triplet peak in the $L_1L_2M_1$ part should also be included when we add spin-orbit coupling. It was also reported that *KLL* spectra are affected by channel mixing, too, though to a smaller degree.[123] We, therefore, expect a better agreement of our *KLL* spectrum in the position and heights of the peaks with experiments as well when our theory accounts for spin-orbit interaction.

Lastly, channel mixing and spin-orbit splitting almost exclusively lead to a redistribution of the partial widths but not to a change of the total width.[120] This is the reason that our total width agreed very well with experiments for argon and hydrogen sulfide.

$L_{2,3}$ -edge Auger spectra

The second part of the L-edge Auger spectrum corresponds to transitions arising from the $1b_1^{-1}$, $3a_1^{-1}$, and $1b_2^{-1}$ core-holes. Experimentally, mostly the Auger transitions to $2b_2^{-2}$ were investigated.[91, 92, 94] The reason is that these are the only transition that lead to a stable non-dissociating final state.[91] It has

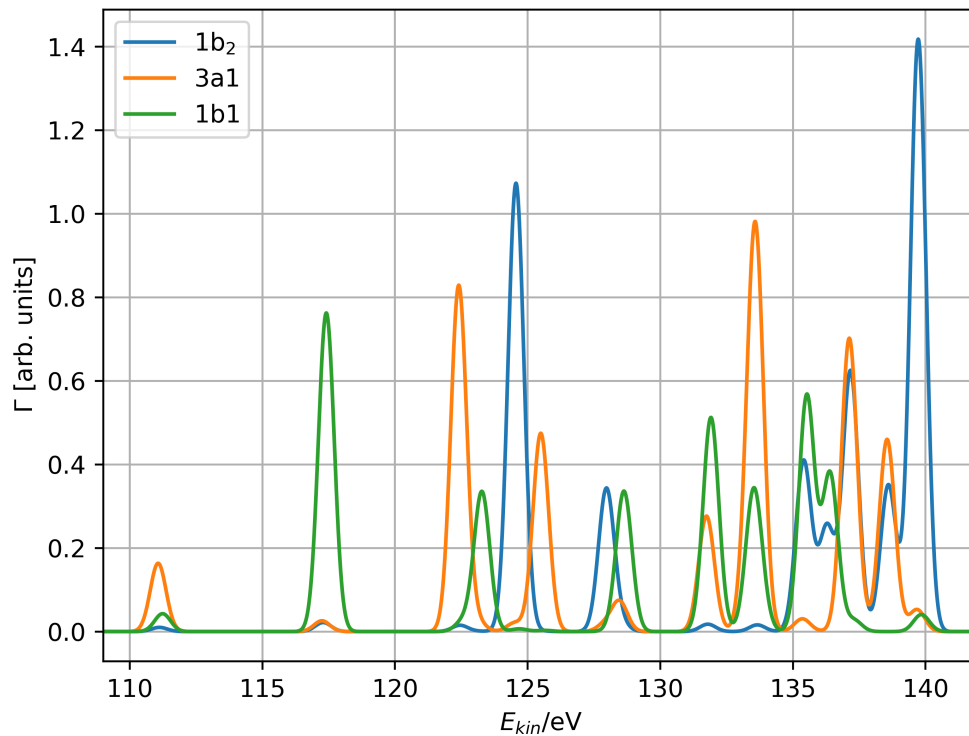


Figure 5: *LMM* Auger spectrum of hydrogen sulfide for the three $2p^{-1}$ holes. Decay width in arbitrary units as a function of the kinetic energy of the emitted electron. The partial widths were calculated with EOM-CCSD and 4(spdf) complex shells. The spectra are normalized to have the same relative sum of widths as in our calculation. Gaussian broadening with FWHM = 0.7 eV.

been suggested that this phenomenon occurs due to the $2b_2$ orbital being the sole valence orbital oriented out of the molecular plane, rendering it nonbonding.[91] These authors also report the relative intensities of the various $\epsilon_Q \rightarrow 2b_2^{-2}$ transitions, with $Q = 1, 2, 3$. Poygin *et al.* reported $0.35 \pm 0.05 : 0.04 \pm 0.01 : 1$ [91] whereas Bueno and coworkers obtained $0.42 \pm 0.03 : 0.09 \pm 0.03 : 1$ experimentally and $0.42 : 0.06 : 1$ theoretically.[92] Our calculated ratio after transforming our decay widths from the irrep basis to the ϵ states basis is $0.41 : 0.06 : 1$ which agrees excellently.

We can explain these ratios as follows. For Auger transitions of a non-s-type hole to be intense, one of the final holes should be parallel-oriented to the initial hole.[124] As the initial hole ϵ_3^{-1} is mostly comprised of $1b_2^{-1}$ and the $1b_2$ orbital is, just as $2b_2$, oriented out of the molecular plane, this respective transition is the most intense. The ϵ_2 orbital has almost no contribution from the $1b_2$ orbital and the corresponding channel is therefore mostly suppressed.

This behavior can also be seen in all other transitions. We can see in our calculated partial widths, that for a channel to be open at least one of the final holes needs the same orientation as the initial hole. The spectra of the different holes therefore look extremely different as can be seen in figure 5. Although the positions of the 16 peaks are also slightly different for the three holes, as they have slightly different ionization potentials, the reason for that is that different channels are open for the different holes. All three holes show seven significant peaks (relative partial width > 0.1) each. For the $1b_1^{-1}$ and $1b_2^{-1}$ holes this is easily explained. There are just seven channels that include the $2b_1$ and $2b_2$ orbital, respectively. In the case of the $3a_1^{-1}$ hole, the channels are open that include the $5a_1$ orbital, which are also seven. The channels that include the $4a_1$ orbital and not the $5a_1$ orbital, however, are not open for this hole. The reason is that the $4a_1$ orbital, despite having the same irrep as the $3a_1^{-1}$ hole and being a valence orbital, still has significant characteristics of a s-orbital. It is thus not parallel oriented to the $3a_1$ hole with p-character. It should be noted that the presented spectra are not measurable because, as discussed, the three orbitals mix to form the three ϵ states. Lastly, we want to point out that, as for the $2s^{-1}$ hole, triplet channels contribute significantly to the total width. The triplet fraction to the sum of widths is 21% ($1b_2^{-1}$), 28% ($3a_1^{-1}$) and 30% ($1b_1^{-1}$).

6 Conclusions

In conclusion, we calculated the total and partial Auger decay widths of the $1s^{-1}$, $2s^{-1}$ and $2p^{-1}$ initial states of hydrogen sulfide and of the $2s^{-1}$ state of argon. We used complex scaling of the Hamiltonian and complex basis functions to describe the emitted electron with L^2 integrable wave functions for argon and H_2S respectively. This work is an extension of this technique to the study of core orbitals from different shells.

For the $1s^{-1}$ hole of H_2S , we found good agreement between the four used methods (CCSD and MP2 with decomposition and EOM-CCSD and EOM-MP2 with Auger channel projectors) and experimental and other theoretical values. We found that EOM-CCSD needs more CBFs to get a comparable sum of partial widths to the other methods. MP2 was used for the first time to calculate Auger widths with CBFs and gives very similar results, especially to CCSD (as both methods use the decomposition procedure), with much less computational costs. In the case of hydrogen sulfide, MP2 is about a factor 10 stronger than CCSD in a typical total and partial width calculation. It should be even more useful for larger molecules and complexes that cannot be tackled by CCSD at all.

Coster-Kronig transitions are present in the Auger decay from the $2s^{-1}$ initial hole in H_2S and Ar. These are extremely strong due to the large spatial overlap of the $2s^{-1}$ hole and the $2p$ electron that fills it, which leads to the very large decay widths of the $2s^{-1}$ states. We saw that additional diffuse complex-scaled shells are needed to properly describe the slow emitted electrons in the Coster-Kronig transitions. In the case of argon we also performed CS calculations with good agreement to CBF, which verifies our approach, even

though the exponents of the additional shells were not fully optimized.

In the Auger decay from the $2p^{-1}$ states of hydrogen sulfide the total widths are one order of magnitude smaller than for the $1s^{-1}$ hole and almost two orders smaller than for the $2s^{-1}$ hole. The reason is that the $2p^{-1}$ hole can only be filled by valence electrons which have a small spatial overlap with the core holes. We found that the three holes $1b_1^{-1}$, $3a_1^{-1}$ and $1b_2^{-1}$ have very different spectra because different channels are open depending on the orientation of the initial hole. The governing rule is that one of the two final states needs to have the same spatial orientation as the initial hole.

We found that EOM-CCSD and EOM-MP2 are the only methods that work for the $2s^{-1}$ and $2p^{-1}$ holes. The latter, however, brings negligible computational benefit. The novel application of MP2 only gives trustworthy results for the holes, where CCSD converges.

In consensus with prior results[46, 84–86] we saw that triplet channels contribute very little to the total Auger width of the $1s^{-1}$ state of H_2S (5% for all four methods). This is different for the other holes. We find that the $2s^{-1}$ Auger width has a triplet contribution of 24% for H_2S and 30% for argon. For the three $2p$ holes of H_2S $1b_2^{-1}$, $3a_1^{-1}$ and $1b_1^{-1}$ we find a triplet share of 21%, 28% and 30%, respectively. The fact that singlet channels are still more important but triplet channels are not negligible in Auger decay from non $1s$ holes agrees with previous results.[125]

As an outlook, we propose the implementation of spin-orbit coupling to the used code to achieve better agreement in the positions and heights of the Auger peaks with experiments. Furthermore, especially more recent experiments were dedicated to the shake structure and vibrational effects in Auger spectra[88, 91, 119, 126], which are also not yet included in our description. Lastly, the potential of MP2 to describe the Auger decay in large molecules, that cannot be described by CCSD due to computational costs, should be explored in the future.

Acknowledgments

T.-C.J. gratefully acknowledges funding from the European Research Council (ERC) under the European Union’s Horizon 2020 research and innovation program (Grant Agreement No. 851766) and the KU Leuven internal funds (Grant No. C14/22/083).

References

- ¹L. Meitner, “Über die entstehung der β -strahl-spektren radioaktiver substanzen”, *Z. Phys.* **9**, 131 (1922).
- ²P. Auger, “Sur les rayons β secondaires produits dans un gaz par des rayons x”, *CR Acad. Sci. (F)* **177**, 169 (1923).
- ³W. Bambynek, B. Crasemann, R. W. Fink, H.-U. Freund, H. Mark, C. D. Swift, R. E. Price, and P. V. Rao, “X-ray fluorescence yields, auger, and coster-kronig transition probabilities”, *Rev. Mod. Phys.* **44**, 716 (1972).
- ⁴A. C. Thompson, D. Vaughan, J. Kirz, D. E. Attwood, E. M. Gullikson, M. R. Howells, K.-J. Kim, J. B. Kortright, I. Lindau, P. Pianetta, A. L. Robinson, J. H. Underwood, G. P. Williams, and H. Winick, *X-ray data booklet* (Lawrence Berkeley National Laboratory, 2009).
- ⁵A. P. Hitchcock, “Bibliography of atomic and molecular inner-shell excitation studies”, *J. Electron Spectrosc.* **67**, 1 (1994).

- ⁶E. E. Rennie, B. Kempgens, H. M. Köppe, U. Hergenbahn, J. Feldhaus, B. S. Itchkawitz, A. L. D. Kilcoyne, A. Kivimäki, K. Maier, M. N. Piancastelli, M. Polcik, A. Rüdell, and A. M. Bradshaw, “A comprehensive photoabsorption, photoionization, and shake-up excitation study of the C 1s cross section of benzene”, *J. Chem. Phys.* **113**, 7362–7375 (2000).
- ⁷S. Carniato, P. Selles, A. Ferté, N. Berrah, A. H. Wuosmaa, M. Nakano, Y. Hikosaka, K. Ito, M. Žitnik, K. Bučar, K. Soejima, D. Jnk, D. Cubaynes, J. M. Bizau, L. Andric, M. A. Khalal, J. Palaudoux, P. Lablanquie, and F. Penent, “Single photon simultaneous K-shell ionization/excitation in C₆H₆: Experiment and theory”, **53**, 244010 (2020).
- ⁸R. Spohr, T. Bergmark, N. Magnusson, L. Werme, C. Nordling, and K. Siegbahn, “Electron spectroscopic investigation of Auger processes in bromine substituted methanes and some hydrocarbons”, **2**, 31 (1970).
- ⁹W. D. Loveland, D. J. Morrissey, and G. T. Seaborg, *Modern nuclear chemistry* (John Wiley & Sons, 2017).
- ¹⁰R. R. Rye and J. E. Houston, “Molecular auger spectroscopy”, **17**, 41–47 (1984).
- ¹¹P. Bolognesi, P. O’Keeffe, Y. Ovcharenko, L. Avaldi, and V. Carravetta, “Resonant auger spectroscopy at the carbon and nitrogen k-edges of pyrimidine”, *J. Chem. Phys.* **136**, 154308 (2012).
- ¹²B. K. Agarwal, *X-ray spectroscopy: an introduction* (Springer, 2013).
- ¹³B. K. McFarland, J. P. Farrell, S. Miyabe, F. Tarantelli, A. Aguilar, N. Berrah, C. Bostedt, J. D. Bozek, P. H. Bucksbaum, J. C. Castagna, R. N. Coffee, J. P. Cryan, L. Fang, R. Feifel, K. J. Gaffney, J. M. Glowia, T. J. Martinez, M. Mucke, B. Murphy, A. Natan, T. Osipov, V. S. Petrović, S. Schorb, T. Schultz, L. S. Spector, M. Swiggers, I. Tenney, S. Wang, J. L. White, W. White, and M. Gühr, “Ultrafast x-ray auger probing of photoexcited molecular dynamics”, *Nat. Commun.* **5**, 4235 (2014).
- ¹⁴K. Ramasesha, S. R. Leone, and D. M. Neumark, “Real-time probing of electron dynamics using attosecond time-resolved spectroscopy”, **67**, 41–63 (2016).
- ¹⁵M. Nisoli, P. Decleva, F. Calegari, A. Palacios, and F. Martín, “Attosecond electron dynamics in molecules”, **117**, 10760–10825 (2017).
- ¹⁶T. Marchenko, L. Inhester, G. Goldsztejn, O. Travnikova, L. Journel, R. Guillemin, I. Ismail, D. Koulentianos, D. Céolin, R. Püttner, M. N. Piancastelli, and M. Simon, “Ultrafast nuclear dynamics in the doubly-core-ionized water molecule observed via Auger spectroscopy”, **98**, 063403 (2018).
- ¹⁷P. Norman and A. Dreuw, “Simulating X-ray spectroscopies and calculating core-excited states of molecules”, *Chem. Rev.* **118**, 7208–7248 (2018).
- ¹⁸P. M. Kraus, M. Zürich, S. K. Cushing, D. M. Neumark, and S. R. Leone, “The ultrafast x-ray spectroscopy revolution in chemical dynamics”, *Nat. Rev. Chem.* **2**, 82 (2018).
- ¹⁹O. Plekan, H. Sa’adeh, A. Ciavardini, C. Callegari, G. Cautero, C. Dri, M. Di Fraia, K. C. Prince, R. Richter, R. Sergo, L. Stebel, M. Devetta, D. Faccialá, C. Vozzi, L. Avaldi, P. Bolognesi, M. C. Castrovilli, D. Catone, M. Coreno, F. Zuccaro, E. Bernes, G. Fronzoni, D. Toffoli, and A. Ponzi, “Experimental and theoretical photoemission study of indole and its derivatives in the gas phase”, **124**, 4115–4127 (2020).
- ²⁰M. Tchapyguine, R. Feifel, R. R. T. Marinho, M. Gisselbrecht, S. L. Sorensen, A. N. de Brito, N. Mårtensson, S. Svensson, and O. Björneholm, “Selective probing of the electronic structure of free clusters using resonant core-level spectroscopy”, **289**, 3–13 (2003).
- ²¹L. A. Harris, “Analysis of materials by electron-excited Auger electrons”, **39**, 1419–1427 (1968).

- ²²S. Hofmann, *Auger- and x-ray photoelectron spectroscopy in materials science: a user-oriented guide*, Vol. 49 (Springer Science & Business Media, 2012).
- ²³P. Zimmermann, S. Peredkov, P. M. Abdala, S. DeBeer, M. Tromp, C. Müller, and J. A. van Bokhoven, “Modern X-ray spectroscopy: XAS and XES in the laboratory”, *Coord. Chem. Rev.* **423**, 213466 (2020).
- ²⁴R. Weissmann and K. Müller, “Auger electron spectroscopy—a local probe for solid surfaces”, **1**, 251–309 (1981).
- ²⁵D. Spanjaard, C. Guillot, M.-C. Desjonqueres, G. Tréglia, and J. Lecante, “Surface core level spectroscopy of transition metals: a new tool for the determination of their surface structure”, *Surf. Sci. Rep.* **5**, 1–85 (1985).
- ²⁶C. J. Powell and M. P. Seah, “Precision, accuracy, and uncertainty in quantitative surface analyses by Auger-electron spectroscopy and x-ray photoelectron spectroscopy”, *J. Vac. Sci. Technol., A* **8**, 735–763 (1990).
- ²⁷T. Orvis, M. Surendran, Y. Liu, A. Cunniff, and J. Ravichandran, “In situ Auger electron spectroscopy of complex oxide surfaces grown by pulsed laser deposition”, *J. Vac. Sci. Technol., A* **37**, 061401 (2019).
- ²⁸Z. Li and U. Becker, “Chemical state effects on the Auger transitions in Cr, Fe, and Cu compounds”, *J. Electron. Spectrosc. and Relat. Phenom.* **237**, 146893 (2019).
- ²⁹L.-C. Chao and S.-H. Yang, “Growth and Auger electron spectroscopy characterization of donut-shaped ZnO nanostructures”, **253**, 7162–7165 (2007).
- ³⁰S. N. Raman, D. F. Paul, J. S. Hammond, and K. D. Bomben, “Auger electron spectroscopy and its application to nanotechnology”, *Microscopy today* **19**, 12–15 (2011).
- ³¹A. I. Kassis, “The amazing world of Auger electrons”, *Int. J. Radiat. Bio.* **80**, 789–803 (2004).
- ³²A. I. Kassis and S. J. Adelstein, “Radiobiologic principles in radionuclide therapy”, *J. Nucl. Med.* **46**, 4S–12S (2005).
- ³³F. Buchegger, F. Perillo-Adamer, Y. M. Dupertuis, and A. Bischof Delaloye, “Auger radiation targeted into DNA: a therapy perspective”, *Eur. J. Nucl. Med. Mol. Imaging* **33**, 1352–1363 (2006).
- ³⁴A. Ku, V. J. Facca, Z. Cai, and R. M. Reilly, “Auger electrons for cancer therapy—a review”, *EJNMMI Radiopharm. Chem.* **4**, 1–36 (2019).
- ³⁵R. W. Howell, “Advancements in the use of auger electrons in science and medicine during the period 2015–2019”, *Int. J. Radiat. Biol.* **99**, 2 (2020).
- ³⁶G. Pirovano, S. A. Jannetti, L. M. Carter, A. Sadique, S. Kossatz, N. Guru, P. Demétrio De Souza França, M. Maeda, B. M. Zeglis, J. S. Lewis, J. L. Humm, and T. Reiner, “Targeted brain tumor radiotherapy using an Auger emitter”, *Clin. Cancer Res.* **26**, 2871–2881 (2020).
- ³⁷J. Borbinha, P. Vaz, and S. Di Maria, “Dosimetric assessment in different tumour phenotypes with Auger electron emitting radionuclides: ^{99m}Tc, ¹²⁵I, ¹⁶¹Tb, and ¹⁷⁷Lu”, *Radiat. Phys. Chem.* **172**, 108763 (2020).
- ³⁸G. Pirovano, T. C. Wilson, and T. Reiner, “Auger: the future of precision medicine”, *Nuclear medicine and biology* **96**, 50–53 (2021).
- ³⁹D. Coster and R. de Laer Kronig, “New type of auger effect and its influence on the x-ray spectrum”, *Physica* **2**, 13 (1935).
- ⁴⁰L. S. Cederbaum, J. Zobeley, and F. Tarantelli, “Giant intermolecular decay and fragmentation of clusters”, *Phys. Rev. Lett.* **79**, 4778 (1997).

- ⁴¹J. Zobeley, R. Santra, and L. S. Cederbaum, “Electronic decay in weakly bound heteroclusters: energy transfer versus electron transfer”, *J. Chem. Phys.* **115**, 5076–5088 (2001).
- ⁴²T. Jahnke, U. Hergenhahn, B. Winter, R. Dörner, U. Fröhling, P. V. Demekhin, K. Gokhberg, L. S. Cederbaum, A. Ehresmann, A. Knie, and A. Dreuw, “Interatomic and intermolecular Coulombic decay”, *Chem. Rev.* **120**, 11295 (2020).
- ⁴³V. Parravicini and T.-C. Jagau, “Interatomic and intermolecular coulombic decay rates from equation-of-motion coupled-cluster theory with complex basis functions”, *J. Chem. Phys.* **159**, 094112 (2023).
- ⁴⁴T. Fransson, Y. Harada, N. Kosugi, N. A. Besley, B. Winter, J. J. Rehr, L. G. M. Pettersson, and A. Nilsson, “X-ray and electron spectroscopy of water”, **116**, 7551–7569 (2016).
- ⁴⁵N. Moiseyev, *Non-hermitian quantum mechanics* (Cambridge University Press, 2011).
- ⁴⁶F. Matz and T.-C. Jagau, “Molecular auger decay rates from complex-variable coupled-cluster theory”, *J. Chem. Phys.* **156**, 114117 (2022).
- ⁴⁷T.-C. Jagau, “Theory of electronic resonances: fundamental aspects and recent advances”, *Chem. Comm.* **58**, 5205 (2022).
- ⁴⁸L. S. Cederbaum, W. Domcke, and J. Schirmer, “Many-body theory of core holes”, *Phys. Rev. A* **22**, 206 (1980).
- ⁴⁹J. Wenzel, M. Wormit, and A. Dreuw, “Calculating core-level excitations and X-ray absorption spectra of medium-sized closed-shell molecules with the algebraic-diagrammatic construction scheme for the polarization propagator”, *J. Comput. Chem.* **35**, 1900 (2014).
- ⁵⁰J. Wenzel, M. Wormit, and A. Dreuw, “Calculating X-ray absorption spectra of open-shell molecules with the unrestricted algebraic-diagrammatic construction scheme for the polarization propagator”, *J. Chem. Theory Comput.* **10**, 4583 (2014).
- ⁵¹S. Coriani and H. Koch, “Communication: x-ray absorption spectra and core-ionization potentials within a core-valence separated coupled cluster framework”, *J. Chem. Phys.* **143**, 181103 (2015).
- ⁵²M. L. Vidal, X. Feng, E. Epifanovsky, A. I. Krylov, and S. Coriani, “New and efficient equation-of-motion coupled-cluster framework for core-excited and core-ionized states”, *J. Chem. Theory Comput.* **15**, 3117–3133 (2019).
- ⁵³J. Liu, D. Matthews, S. Coriani, and L. Cheng, “Benchmark calculations of K-edge ionization energies for first-row elements using scalar-relativistic core–valence-separated equation-of-motion coupled-cluster methods”, *J. Chem. Theory Comput.* **15**, 1642–1651 (2019).
- ⁵⁴S. Bari, L. Inhester, K. Schubert, K. Mertens, J. O. Schunck, S. Dörner, S. Deinert, L. Schwob, S. Schippers, A. Müller, S. Klumpp, and M. Martins, “Inner-shell x-ray absorption spectra of the cationic series nh_y^+ ($y = 0-3$)”, *Phys. Chem. Chem. Phys.* **21**, 16505 (2019).
- ⁵⁵F. Frati, F. de Groot, J. Cerezo, F. Santoro, L. Cheng, R. Faber, and S. Coriani, “Coupled cluster study of the x-ray absorption spectra of formaldehyde derivatives at the oxygen, carbon, and fluorine K-edges”, *J. Chem. Phys.* **151**, 064107 (2019).
- ⁵⁶X. Zheng and L. Cheng, “Performance of delta-coupled-cluster methods for calculations of core-ionization energies of first-row elements”, *J. Chem. Theory Comput.* **15**, 4945–4955 (2019).

- ⁵⁷K. D. Nanda, M. L. Vidal, R. Faber, S. Coriani, and A. I. Krylov, “How to stay out of trouble in RIXS calculations within equation-of-motion coupled-cluster damped response theory? Safe hitchhiking in the excitation manifold by means of core–valence separation”, *Phys. Chem. Chem. Phys.* **22**, 2629–2641 (2020).
- ⁵⁸S. I. Bokarev and O. Kühn, “Theoretical x-ray spectroscopy of transition metal compounds”, *WIREs Computational Molecular Science* **10**, e1433 (2020).
- ⁵⁹T. Fransson, I. E. Brumboiu, M. L. Vidal, P. Norman, S. Coriani, and A. Dreuw, “XABOOM: an X-ray absorption benchmark of organic molecules based on carbon, nitrogen, and oxygen $1s \rightarrow \pi^*$ transitions”, *J. Chem. Theory Comput.* **17**, 1618 (2021).
- ⁶⁰T. W. Gorczyca, “Auger decay of the photoexcited $1s^{-1}np$ rydberg series in neon”, *Phys. Rev. A* **61**, 024702 (2000).
- ⁶¹J. García, T. R. Kallman, M. Witthoef, E. Behar, C. Mendoza, P. Palmeri, P. Quinet, M. A. Bautista, and M. Klapisch, “Nitrogen K-shell photoabsorption”, *Astrophys. J. Suppl. S.* **185**, 477–485 (2009).
- ⁶²J. Tennyson, “Electron–molecule collision calculations using the r-matrix method”, *Phys. Rep.* **491**, 29 (2010).
- ⁶³U. Fano, “Effects of configuration interaction on intensities and phase shifts”, *Phys. Rev.* **124**, 1866 (1961).
- ⁶⁴H. Feshbach, “A unified theory of nuclear reactions. ii”, *Annals of Physics* **19**, 287 (1962).
- ⁶⁵P.-O. Löwdin, “Studies in perturbation theory. iv. solution of eigenvalue problem by projection operator formalism”, *Journal Math. Phys.* **3**, 969 (1962).
- ⁶⁶V. Averbukh and L. S. Cederbaum, “Ab initio calculation of interatomic decay rates by a combination of the Fano ansatz, Green’s-function methods, and the Stieltjes imaging technique”, *J. Chem. Phys.* **123**, 204107 (2005).
- ⁶⁷L. Inhester, C. F. Burmeister, G. Groenhof, and H. Grubmüller, “Auger spectrum of a water molecule after single and double core ionization”, *J. Chem. Phys.* **136**, 144304 (2012).
- ⁶⁸L. Inhester, C. F. Burmeister, G. Groenhof, and H. Grubmüller, “Erratum: “Auger spectrum of a water molecule after single and double core ionization” [*J. Chem. Phys.* 136, 144304 (2012)]”, *J. Chem. Phys.* **141**, 069904 (2014).
- ⁶⁹P. Kolorenč and V. Averbukh, “Fano-ADC(2,2) method for electronic decay rates”, *J. Chem. Phys.* **152**, 214107 (2020).
- ⁷⁰W. Skomorowski and A. I. Krylov, “Feshbach–fano approach for calculation of auger decay rates using equation-of-motion coupled-cluster wave functions. i. theory and implementation”, *J. Chem. Phys.* **154**, 084124 (2021).
- ⁷¹W. Skomorowski and A. I. Krylov, “Feshbach–Fano approach for calculation of Auger decay rates using equation-of-motion coupled-cluster wave functions. II. Numerical examples and benchmarks”, *J. Chem. Phys.* **154**, 084125 (2021).
- ⁷²B. N. C. Tenorio, T. A. Voß, S. I. Bokarev, P. Decleva, and S. Coriani, “Multireference approach to normal and resonant auger spectra based on the one-center approximation”, *J. Chem. Theory Comput.* **18**, 4387 (2022).
- ⁷³J. Aguilar and J.-M. Combes, “A class of analytic perturbations for one-body schrödinger hamiltonians”, *Commun. Math. Phys.* **22**, 269 (1971).

- ⁷⁴E. Balslev and J.-M. Combes, “Spectral properties of many-body Schrödinger operators with dilatation-analytic interactions”, *Commun. Math. Phys.* **22**, 280 (1971).
- ⁷⁵C. W. McCurdy Jr and T. N. Rescigno, “Extension of the method of complex basis functions to molecular resonances”, *Phys. Rev. Lett.* **41**, 1364 (1978).
- ⁷⁶N. Moiseyev and C. Corcoran, “Autoionizing states of H_2 and H_2^- using the complex-scaling method”, *Phys. Rev. A* **20**, 814–817 (1979).
- ⁷⁷K. B. Bravaya, D. Zuev, E. Epifanovsky, and A. I. Krylov, “Complex-scaled equation-of-motion coupled-cluster method with single and double substitutions for autoionizing excited states: theory, implementation, and examples”, *J. Chem. Phys.* **138**, 124106 (2013).
- ⁷⁸T.-C. Jagau, D. Zuev, K. B. Bravaya, E. Epifanovsky, and A. I. Krylov, “A fresh look at resonances and complex absorbing potentials: density matrix-based approach”, *J. Phys. Chem. Lett.* **5**, 310–315 (2014).
- ⁷⁹D. Zuev, T.-C. Jagau, K. B. Bravaya, E. Epifanovsky, Y. Shao, E. Sundstrom, M. Head-Gordon, and A. I. Krylov, “Complex absorbing potentials within EOM-CC family of methods: theory, implementation, and benchmarks”, *J. Chem. Phys.* **141**, 024102 (2014).
- ⁸⁰A. F. White, M. Head-Gordon, and C. W. McCurdy, “Complex basis functions revisited: Implementation with applications to carbon tetrafluoride and aromatic N-containing heterocycles within the static-exchange approximation”, *J. Chem. Phys.* **142**, 054103 (2015).
- ⁸¹A. F. White, C. W. McCurdy, and M. Head-Gordon, “Restricted and unrestricted non-Hermitian Hartree-Fock: theory, practical considerations, and applications to metastable molecular anions”, *J. Chem. Phys.* **143**, 074103 (2015).
- ⁸²A. F. White, E. Epifanovsky, C. W. McCurdy, and M. Head-Gordon, “Second order Møller-Plesset and coupled cluster singles and doubles methods with complex basis functions for resonances in electron-molecule scattering”, *J. Chem. Phys.* **146**, 234107 (2017).
- ⁸³T.-C. Jagau, K. B. Bravaya, and A. I. Krylov, “Extending quantum chemistry of bound states to electronic resonances”, 525 (2017).
- ⁸⁴F. Matz and T.-C. Jagau, “Channel-specific core-valence projectors for determining partial auger decay widths”, *Mol. Phys.* **121**, e2105270 (2023).
- ⁸⁵F. Matz, J. Nijssen, and T.-C. Jagau, “Ab initio investigation of the auger spectra of methane, ethane, ethylene, and acetylene”, *J. Phys. Chem. A* **127**, 6147 (2023).
- ⁸⁶N. K. Jayadev, A. Ferino-Pérez, F. Matz, A. I. Krylov, and T.-C. Jagau, “The auger spectrum of benzene”, *J. Chem. Phys.* **158**, 064109 (2023).
- ⁸⁷K. Faegri Jr and O. Keski-Rahkonen, “Sulphur kll auger spectra of gaseous sulphur compounds”, *J. Electron Spectrosc.* **11**, 275 (1977).
- ⁸⁸R. Püttner, D. Céolin, R. Guillemin, R. K. Kushawaha, T. Marchenko, L. Journel, M. N. Piancastelli, and M. Simon, “Detailed analysis of shake structures in the kll auger spectrum of h_2s ”, *Phys. Rev. A* **93**, 042501 (2016).
- ⁸⁹L. Asplund, P. Kelfve, B. Blomster, H. Siegbahn, K. Siegbahn, R. L. Lozes, and U. I. Wahlgren, “Molecular auger electron spectra of second row elements. sulfur compounds”, *Phys. Scripta* **16**, 273 (1977).
- ⁹⁰Y. Hikosaka, P. Lablanquie, F. Penent, J. G. Lambourne, R. I. Hall, T. Aoto, and K. Ito, “Sub-natural linewidth auger electron spectroscopy of the 2s hole decay in h_2s ”, *J. Electron Spectrosc.* **137**, 287 (2004).

- ⁹¹M. Poygin, R. Püttner, M. Martins, V. Pennanen, M. Jurvansuu, Y. H. Jiang, H. Aksela, S. Aksela, and G. Kaindl, “Detailed study of the $s\ 2p^{-1} \rightarrow x\ a_1\ (2b_1^{-2})$ normal auger spectra of h_2s ”, *Phys. Rev. A* **74**, 012711 (2006).
- ⁹²A. M. Bueno, A. N. de Brito, R. F. Fink, M. Bässler, O. Björneholm, F. Burmeister, R. Feifel, C. Miron, S. L. Sorensen, H. Wang, and S. Svensson, “Influence of chemical bonds on the lifetime of the molecular-field-split $2p$ levels in h_2s ”, *Phys. Rev. A* **67**, 022714 (2003).
- ⁹³S. Svensson, A. N. de Brito, M. P. Keane, N. Correia, and L. Karlsson, “Observation of an energy shift in the $s2p_{3/2}$ – $s2p_{1/2}$ spin-orbit splitting between x-ray photoelectron and auger-electron spectra for the h_2s molecule”, *Phys. Rev. A* **43**, 6441 (1991).
- ⁹⁴S. Svensson, A. Ausmees, S. J. Osborne, G. Bray, F. Gel’mukhanov, H. Ågren, A. N. de Brito, O.-P. Sairanen, A. Kivimäki, E. Nömmiste, H. Aksela, and S. Aksela, “Observation of an anomalous decay ratio between the molecular field split levels in the $s\ 2p$ core photoelectron and lvv auger spectrum of h_2s ”, *Phys. Rev. Lett.* **72**, 3021 (1994).
- ⁹⁵R. J. Bartlett and I. Shavitt, *Many-body methods in chemistry and physics: MBPT and coupled-cluster theory* (Cambridge University Press, 2009).
- ⁹⁶J. F. Stanton and R. J. Bartlett, “The equation of motion coupled-cluster method. A systematic biorthogonal approach to molecular excitation energies, transition probabilities, and excited state properties”, *J. Chem. Phys.* **98**, 7029 (1993).
- ⁹⁷R. J. Bartlett, “Coupled-cluster theory and its equation-of-motion extensions”, *WIREs Comput. Mol. Sci.* **2**, 126 (2012).
- ⁹⁸K. Sneskov and O. Christiansen, “Excited state coupled cluster methods”, *WIREs Comput. Mol. Sci.* **2**, 566 (2012).
- ⁹⁹J. F. Stanton and J. Gauss, “Perturbative treatment of the similarity transformed hamiltonian in equation-of-motion coupled-cluster approximations”, *J. Chem. Phys.* **103**, 1064 (1995).
- ¹⁰⁰K. W. Sattelmeyer, H. F. Schaefer, and J. F. Stanton, “Use of $2h$ and $3h$ - p like coupled-cluster Tamm-Dancoff approaches for the equilibrium properties of ozone”, **378**, 42–46 (2003).
- ¹⁰¹J. Shen and P. Piecuch, “Doubly electron-attached and doubly ionized equation-of-motion coupled-cluster methods with 4-particle-2-hole and 4-hole-2-particle excitations and their active-space extensions”, **138**, 194102 (2013).
- ¹⁰²D. Bokhan, D. N. Trubnikov, A. Perera, and R. J. Bartlett, “Explicitly-correlated double ionization potentials and double electron attachment equation-of-motion coupled cluster methods”, **692**, 191–195 (2018).
- ¹⁰³F. Weigend, M. Häser, H. Patzelt, and R. Ahlrichs, “Ri-mp2: optimized auxiliary basis sets and demonstration of efficiency”, *Chem. Phys. Lett.* **294**, 143 (1998).
- ¹⁰⁴E. Z. Chelkowska and F. P. Larkins, “Auger spectroscopy for molecules: tables of matrix elements for transition-rate calculations corresponding to an s -, p -, or d -type initial hole”, *Atom. Data Nucl. Data* **49**, 121 (1991).

- ¹⁰⁵E. Epifanovsky, A. T. B. Gilbert, X. Feng, J. Lee, Y. Mao, N. Mardirossian, P. Pokhilko, A. F. White, M. P. Coons, A. L. Dempwolff, Z. Gan, D. Hait, P. R. Horn, L. D. Jacobson, I. Kaliman, J. Kussmann, A. W. Lange, K. U. Lao, D. S. Levine, J. Liu, S. C. McKenzie, A. F. Morrison, K. D. Nanda, F. Plasser, D. R. Rehn, M. L. Vidal, Z.-Q. You, Y. Zhu, B. Alam, B. J. Albrecht, A. Aldossary, E. Alguire, J. H. Andersen, V. Athavale, D. Barton, K. Begam, A. Behn, N. Bellonzi, Y. A. Bernard, E. J. Berquist, H. G. A. Burton, A. Carreras, K. Carter-Fenk, R. Chakraborty, A. D. Chien, K. D. Closser, V. Cofer-Shabica, S. Dasgupta, M. de Wergifosse, J. Deng, M. Diedenhofen, H. Do, S. Ehlert, P.-T. Fang, S. Fatehi, Q. Feng, T. Friedhoff, J. Gayvert, Q. Ge, G. Gidofalvi, M. Goldey, J. Gomes, C. E. González-Espinoza, S. Gulania, A. O. Gunina, M. W. D. Hanson-Heine, P. H. P. Harbach, A. Hauser, M. F. Herbst, M. H. Vera, M. Hodecker, Z. C. Holden, S. Houck, X. Huang, K. Hui, B. C. Huynh, M. Ivanov, Ádám Jász, H. Ji, H. Jiang, B. Kaduk, S. Kähler, K. Khistyayev, J. Kim, G. Kis, P. Klunzinger, Z. Koczor-Benda, J. H. Koh, D. Kosenkov, L. Koulias, T. Kowalczyk, C. M. Krauter, K. Kue, A. Kunitsa, T. Kus, I. Ladjászki, A. Landau, K. V. Lawler, D. Lefrancois, S. Lehtola, R. R. Li, Y.-P. Li, J. Liang, M. Liebenthal, H.-H. Lin, Y.-S. Lin, F. Liu, K.-Y. Liu, M. Loipersberger, A. Luenser, A. Manjanath, P. Manohar, E. Mansoor, S. F. Manzer, S.-P. Mao, A. V. Marenich, T. Markovich, S. Mason, S. A. Maurer, P. F. McLaughlin, M. F. S. J. Menger, J.-M. Mewes, S. A. Mewes, P. Morgante, J. W. Mullinax, K. J. Oosterbaan, G. Paran, A. C. Paul, S. K. Paul, F. Pavošević, Z. Pei, S. Prager, E. I. Proynov, Ádám Rák, E. Ramos-Cordoba, B. Rana, A. E. Rask, A. Rettig, R. M. Richard, F. Rob, E. Rossomme, T. Scheele, M. Scheurer, M. Schneider, N. Sergueev, S. M. Sharada, W. Skomorowski, D. W. Small, C. J. Stein, Y.-C. Su, E. J. Sundstrom, Z. Tao, J. Thirman, G. J. Tornai, T. Tsuchimochi, N. M. Tubman, S. P. Veccham, O. Vydrov, J. Wenzel, J. Witte, A. Yamada, K. Yao, S. Yeganeh, S. R. Yost, A. Zech, I. Y. Zhang, X. Zhang, Y. Zhang, D. Zuev, A. Aspuru-Guzik, A. T. Bell, N. A. Besley, K. B. Bravaya, B. R. Brooks, D. Casanova, J.-D. Chai, S. Coriani, C. J. Cramer, G. Cserey, A. E. DePrince, R. A. DiStasio, A. Dreuw, B. D. Dunietz, T. R. Furlani, W. A. Goddard, S. Hammes-Schiffer, T. Head-Gordon, W. J. Hehre, C.-P. Hsu, T.-C. Jagau, Y. Jung, A. Klamt, J. Kong, D. S. Lambrecht, W. Liang, N. J. Mayhall, C. W. McCurdy, J. B. Neaton, C. Ochsenfeld, J. A. Parkhill, R. Peverati, V. A. Rassolov, Y. Shao, L. V. Slipchenko, T. Stauch, R. P. Steele, J. E. Subotnik, A. J. W. Thom, A. Tkatchenko, D. G. Truhlar, T. V. Voorhis, T. A. Wesolowski, K. B. Whaley, H. L. Woodcock, P. M. Zimmerman, S. Faraji, P. M. W. Gill, M. Head-Gordon, J. M. Herbert, and A. I. Krylov, “Software for the frontiers of quantum chemistry: an overview of developments in the Q-Chem 5 package”, *J. Chem. Phys.* **155**, 084801 (2021).
- ¹⁰⁶P. Wang, T. X. Carroll, T. D. Thomas, L. J. Sæthre, and K. J. Børve, “Calibration of oxygen 1s ionization energies. accurate energies for co₂, h₂o, co, and o₂”, *Journal of Electron Spectroscopy and Related Phenomena* **251**, 147103 (2021).
- ¹⁰⁷M. Breinig, M. H. Chen, G. E. Ice, F. Parente, B. Crasemann, and G. S. Brown, “Atomic inner-shell level energies determined by absorption spectrometry with synchrotron radiation”, *Phys. Rev. A* **22**, 520 (1980).
- ¹⁰⁸P. Glans, R. E. LaVilla, M. Ohno, S. Svensson, G. Bray, N. Wassdahl, and J. Nordgren, “Determination of the lifetime width of the argon l₁-hole state”, *Phys. Rev. A* **47**, 1539 (1993).
- ¹⁰⁹O. Keski-Rahkonen and M. O. Krause, “Total and partial atomic-level widths”, *Atom. Data Nucl. Data* **14**, 139 (1974).
- ¹¹⁰M. O. Krause and J. H. Oliver, “Natural widths of atomic k and l levels, k α x-ray lines and several kll auger lines”, *J. Phys. Chem. Ref. Data* **8**, 329 (1979).
- ¹¹¹M. H. Chen and B. Crasemann, “K- l l auger transition probabilities for elements with low and intermediate atomic numbers”, *Phys. Rev. A* **8**, 7 (1973).

- ¹¹²P Weightman, “X-ray-excited auger and photoelectron spectroscopy”, *Electronic Properties of Surfaces*, 135–195 (2018).
- ¹¹³W. Mehlhorn and W. N. Asaad, “Das kll-auger-spektrum für $10 \leq z \leq 36$ ”, *Z. Phys.* **191**, 231 (1966).
- ¹¹⁴T. Kylli, J. Karvonen, H. Aksela, A. Kivimäki, S. Aksela, R. Camilloni, L. Avaldi, M. Coreno, M. De Simone, R. Richter, K. C. Prince, and S. Stranges, “ L_1 - $L_{2,3}$ m coster-kronig transitions in argon”, *Phys. Rev. A* **59**, 4071 (1999).
- ¹¹⁵P. Lablanquie, S.-M. Huttula, M. Huttula, L. Andric, J. Palaudoux, J. H. D. Eland, Y. Hikosaka, E. Shigemasa, K. Ito, and F. Penent, “Multi-electron spectroscopy: auger decays of the argon 2s hole”, *Phys. Chem. Chem. Phys.* **13**, 18355 (2011).
- ¹¹⁶G. N. Ogurtsov, I. P. Flaks, and S. V. Avakyan, “Auto-ionization states in argon”, *Sov. Phys. JETP* **30**, 16 (1969).
- ¹¹⁷P. Lablanquie, F. Penent, R. I. Hall, H. Kjeldsen, J. H. D. Eland, A. Muehleisen, P. Pelicon, Z. Šmit, M. Zitnik, and F. Koike, “Coster-kronig decay of the ar 2s hole observed by auger-threshold photoelectron coincidence spectroscopy”, *Phys. Rev. Lett.* **84**, 47 (2000).
- ¹¹⁸L. Avaldi, J. J. Jureta, and B. P. Marinković, “Energy analysis of ejected electrons in the region of the ar L_1 - $L_{2,3}$ m coster-kronig transitions (25–56 eV) induced by electron impact”, *J. Electron Spectrosc.* **237**, 146898 (2019).
- ¹¹⁹J. Pedersen, P. Decleva, S. Coriani, and B. N. C. Tenorio, “Description of the kll auger–meitner decay spectra of argon following primary and satellite core-ionized states”, *J. Chem. Phys.* **159** (2023).
- ¹²⁰K. R. Karim and B. Crasemann, “Continuum interaction in low-energy radiationless transitions”, *Phys. Rev. A* **31**, 709 (1985).
- ¹²¹K. R. Karim and B. Crasemann, “ L_1 - $L_{2,3} m_1$ coster-kronig spectrum of argon in intermediate coupling”, *Phys. Rev. A* **30**, 1107 (1984).
- ¹²²J. Bruneau, “Mcdf calculation of argon auger process”, *J. Phys. B: At. Mol. Phys.* **16**, 4135 (1983).
- ¹²³G. Howat, T. Aberg, and O. Goscinski, “Relaxation and final-state channel mixing in the auger effect”, *J. Phys. B: At. Mol. Phys.* **11**, 1575 (1978).
- ¹²⁴F. Gel’ mukhanov, H. Ågren, S. Svensson, H. Aksela, and S. Aksela, “Theory of auger spectra for molecular-field-split core levels”, *Phys. Rev. A* **53**, 1379 (1996).
- ¹²⁵U. Alkemper and F. Von Busch, “Auger and electron/double-ion coincidence spectroscopy of sulfur (2p)-ionized CS_2 molecules”, *J. Elec. Spectrosc.* **93**, 115 (1998).
- ¹²⁶Z. Bao, R. F. Fink, O. Travnikova, D. Céolin, S. Svensson, and M. N. Piancastelli, “Detailed theoretical and experimental description of normal auger decay in O_2 ”, *J. Phys. B: At. Mol. Opt.* **41**, 125101 (2008).